Multitemporal Spaceborne SAR Data for Urban Change Detection in China

Yifang Ban, *Member, IEEE*, and Osama A. Yousif

***Abstract*—The objective of this research is to examine effective methods for urban change detection using multitemporal spaceborne SAR data in two rapid expanding cities in China. One scene of ERS-2 SAR C-VV image was acquired in Beijing in 1998 and in shanghai in 1999 respectively and one scene of ENVISAT ASAR C-VV image was acquired in near-anniversary dates in 2008 in Beijing and Shanghai. To compare the SAR images from different dates, a modified ratio operator that takes into account both positive and negative changes was developed to derive a change image. A generalized version of Kittler-Illingworth minimum-error thresholding algorithm was then tested to automatically classify the change image into two classes, change and no change. Various probability density functions such as Log normal, Generalized Gaussian, Nakagami ratio, and Weibull ratio were investigated to model the distribution of the change and no change classes. The results showed that Kittler-Illingworth algorithm applied to the modified ratio image is very effective in detecting temporal changes in urban areas using SAR images. Log normal and Nakagami density models achieved the best results. The Kappa coefficients of these methods were of 0.82 and 0.71 for Beijing and Shanghai respectively while the false alarm rates were 2.7% and 4.75%. The findings indicated that the change accuracies obtained using Kittler-Illingworth algorithm vary depending on how the assumed conditional class density function fits the histograms of change and no change classes.**

***Index Terms*—Change detection, ENVISAT ASAR, ERS-2 SAR, minimum-error thresholding, modified ratio, multitemporal, urbanization.**

I. Introduction

CHINA, the most populous country on Earth, has experienced rapid urbanization due to an unprecedented combination of economic and population growth since the early 1980s. Two decades ago, fewer than 20% of China's people lived in urban areas; today it is approximately 50%; and by 2020 it is expected to be 60%. It is projected that China's urban population will increase 350 million by 2025 with 219 cities having a population over 1 million (compared to 35 cities in Europe) [1]. Urbanization and the impact of human settlements are two of the main causes of global environmental degradation. Development associated with urban sprawl not only decreases the amount of agricultural land, forests, grassland, wetlands, and open space but also disrupts ecosystems and fragment habitats. Urban sprawl is one of the major factors causing air pollution, since the car-dependent lifestyle imposed by sprawl leads to increases in fossil fuel consumption and emissions of greenhouse gases [2], [3]. Therefore, monitoring urbanization and their impact on the environment is of critical importance for urban planning & sustainable development in China.

Most of the efforts in China for urbanization monitoring are based on optical remote sensing, e.g., [4]–[10]. Due to frequent cloud cover, smog, haze and sand storms, however, optical data may not be available during critical monitoring cycles. Multitemporal SAR images, on the other hand, have been increasingly used in change detection studies [11]–[30] due to SAR's independence of atmospheric and solar illumination conditions and its unique information content [13]. For examples, [12] and [13] performed unsupervised change detection using a generalized Kittler-Illingworth minimum error thresholding algorithm to account for the non-Gaussian distribution of SAR images. [14] investigated four different types of change variables computed from multitemporal SAR images for the purpose of change detection. [15] combined feature-based and pixel-based techniques for change detection in urban areas and found the method to be effective, irrespectively of misregistration errors due to reprojection problems or difference in the sensor's viewing geometry, which are common in multitemporal SAR images. [16] investigated multitemporal RADARSAT-1 SAR for urban land-cover mapping and change detection in the Greater Toronto Area using a supervised method. In [17], Time-Series InSAR data were used to monitor subsidence and landslides in urban areas, analyze cities growth and measure the deformation of large man-made structures in China.

With the launches of ESA's ENVISAT ASAR, Canada's RADARSAT-2 SAR, JAXA's ALOS PalSAR and DLR's Terra SAR-X, multitemporal SAR data are routinely available worldwide, thus providing an excellent opportunity for change detection studies in many fast growing cities and regions in the world. Therefore, the objective of this research is to investigate multitemporal, single-frequency, single-polarization ENVISAT ASAR and ERS-2 SAR images for change detection in China using unsupervised change detection algorithms.

II. Methodology

The overview of the methodology using multitemporal SAR data for urban change detection is presented in Fig. 1. The details of the method are discussed in sections below.

Manuscript received October 31, 2011; revised March 15, 2012; accepted April 10, 2012. Date of publication July 03, 2012; date of current version July 20, 2012. This work was supported by the Swedish National Space Board. The research is also part of the project "Satellite Monitoring of Urbanization for Sustainable Urban Development" within the European Space Agency (ESA) and the Chinese Ministry of Science and Technology (MOST)'s Dragon II program.

The authors are with the Division of Geoinformatics, Royal Institute of Technology–KTH, Stockholm, Sweden (corresponding author e-mail: yifang@kth.se).

Color versions of one or more of the figures in this paper are available online at http://ieeexplore.ieee.org.

Digital Object Identifier 10.1109/JSTARS.2012.2201135

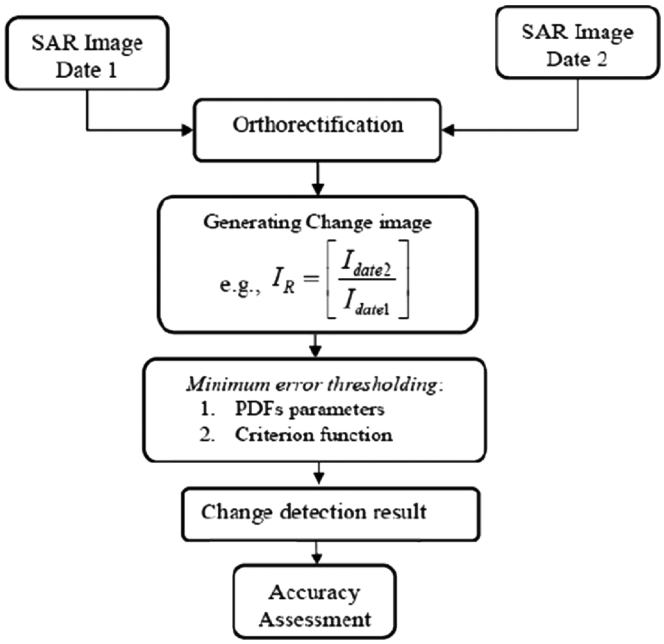

Fig. 1. Methodology flowchart.

A. Image Pre-Processing

1) Orthorectification of SAR Data: To correct for relief displacement and bring the multitemporal SAR images together, all SAR images were orthorectified to WGS 84 datum with UTM projection using a satellite orbital model and a SRTM DEM.

2) Speckle Filtering: The existence of the multiplicative speckle noise in SAR images, affects the ability of the algorithm to separate change and no change classes. To maximize the discrimination capability between change and no change classes, a pre-processing step is required to remove this noise in SAR images. Enhanced Lee filter with window size of 7 × 7 was used to remove the speckle noise. Earlier experiment results showed that two iterations of this filter produced the best result in terms of the achievable accuracy [18].

B. Unsupervised Change Detection

Unsupervised change detection usually involves two steps. First, the multitemporal co-registered images are used to generate a change image that accentuates the intensity in changed areas. Several operators have been tested and among them, image differencing (ID) and its extension change vector analysis (CVA), have been used extensively in change detection using optical data. Recently, Kullback-Leibler divergence, that measures distance between two probability density functions estimated locally, was also examined as a change indicator [19]. Regarding SAR data, the existence of multiplicative speckle noise makes the use of ID inappropriate thus image rationing is preferred for generating change variable image, since at least theoretically it has the important property of eliminating speckle noise [12], [13], [20]. The second step is the automatic thresholding of the change variable image. Several thresholding algorithms were proposed including Kittler-Illingworth minimum error thresholding algorithm, Otsu's algorithm, and Wang's algorithm [21]. Among them, minimum error thresholding is the most commonly used unsupervised change detection algorithm [21]. This algorithm has been applied successfully to both multitemporal optical data [21] and multitemporal SAR images after introducing some modifications [13] and [14].

Based on Bayesian decision theory, Kittler & Illingworth developed the minimum error thresholding algorithm to automatically separate objects from the background in a generic type image [22]. The algorithm uses a histogram-fitting technique to estimate the unknown probability density function parameters. [13] and [23] applied the algorithm to change detection studies using multitemporal SAR images. However, their findings indicated the need to explore different probability density functions suitable for fitting the ratio image derived from multitemporal SAR images. [23] successfully applied the method to multitemporal RADARSAT-1 SAR images using the log-ratio approach to generate the change image. The main drawback associated with using Kittler-Illingworth minimum error thresholding algorithm is the fact that selecting more than a single threshold is computationally expensive. However, [24] proposed a modified double-thresholding Kittler-Illingworth algorithm that utilizes a properly defined cost-function. This cost-function is the minimum value of the criterion function adopted to select the decision threshold in the log-ratio image assuming a generalized Gaussian model.

In this research, a modified ratio operator that takes into account both positive and negative changes was examined by comparing the multitemporal SAR images on a pixel-by-pixel basis. Various probability density functions such as Generalized Gaussian (GG), Log normal (LN), Nakagami ratio (NR), and Weibull ratio (WR) models were tested to model the distribution of the change and no change classes. The detailed methodology is described in the following sections.

1) Modified Ratio Operator: Let us assume that we have two co-registered multitemporal SAR amplitude images acquired at time t_1 and t_2 respectively:

$$X_1 = \left\{x_1^{ij}, i : 1 \ldots n, j : 1 \ldots m\right\}$$
$$X_2 = \left\{x_2^{ij}, i : 1 \ldots n, j : 1 \ldots m\right\} \quad (1)$$

Our purpose is to automatically find areas that have changed over time by comparing these two images on a pixel by pixel basis. For SAR images, the ratio operator is often used to generate the change image since it will eliminate the speckle noise assuming this noise is multiplicative and reproduced in repeat-pass images [12]. In [14], the authors found the ratio operator to be more suitable than second and third cumulants when it comes to detecting sharp changes such as those associated with urban areas. In [24], a neighborhood-based ratio operator was developed in order to further reduce the effect of speckle thus improve change detection. In this study a modified version of the ratio operator will be used to generate the change image. Unlike the ratio operator, the modified ratio operator clusters both positive and negative changes together in one side of the histogram, which in turn allows using a single threshold approach to detect both types of changes simultaneously. This operator takes into account the relationship between the intensities in first and

second date images and generates a ratio that is always greater than or equal to one as shown in (2).

$$\mathrm{r_{ij}} = \frac{\max\left(x_1^{\mathrm{ij}}, x_2^{\mathrm{ij}}\right)}{\min\left(x_1^{\mathrm{ij}}, x_2^{\mathrm{ij}}\right)} \tag{2}$$

This operator transfers changed pixels with intensity decrease to the same side of the histogram as changed pixels with intensity increase. By clustering both positive and negative changes into one side of the histogram, the prior probability of change class will increase. This will consequently improve the histogram-based estimation of its conditional density function. After the identification of changed areas, the separation of positive changes from negative changes can easily be done by comparing the original amplitudes $\mathrm{x_1^{ij}}$ and $\mathrm{x_2^{ij}}$.

2) Minimum Error Thresholding Algorithm: Unsupervised change detection can be viewed as a binary classification problem with only two possible states of nature (change and no change) (Fig. 2). If the prior probabilities and probability density functions of change and no change classes are known in advance, then Bayesian decision rule can be used to threshold the change variable into two possible classes in a way that minimizes the probability of classification error [31]. In unsupervised change detection, however, the above mentioned information is neither known nor can be directly estimated as no training data exists. [22] proposed an algorithm that simultaneously estimates the unknown probabilities and locates an optimum threshold $\mathrm{r^*}$ that can be used to classify each pixel in the change image into one of two possible classes:

$$\begin{aligned} &\text{If } \mathrm{r_{ij}} \leq \mathrm{r^*} \\ &\text{Then } \mathrm{r_{ij}} \rightarrow \text{No Change Class} \\ &\text{Else } \mathrm{r_{ij}} \rightarrow \text{Change Class} \end{aligned}$$

The statistical properties of the change image generated from the modified ratio operator can be summarized by constructing a normalized histogram h(r) consisting of L quantization levels. This histogram is a good approximation of the probability density p(r) of the modified ratio image. According to total probability theorem, this probability density p(r) is a result of the combination of two different populations (change and no change):

$$p(r) = P_1 p_1(r) + P_2 p_2(r) \tag{3}$$

where $\mathrm{P_1}$ and $\mathrm{P_2}$ are the prior probabilities of no change and change classes respectively, and $\mathrm{p_1(r)}$, $\mathrm{p_2(r)}$ are their conditional density functions. Given an arbitrary selected threshold $\mathrm{r_T}$ from all possible threshold values (T ranges from 1 to L) that divides the histogram into two classes, it is possible to use each of these histogram sections to estimate the unknown probabilities. First the prior probabilities can be estimated simply from the normalized histogram using (4).

$$P_1 = \sum_{\mathrm{r=r_1}}^{\mathrm{r_T}} h(r) \quad \text{and} \quad P_2 = \sum_{\mathrm{r=r_{T+1}}}^{\mathrm{r_L}} h(r) \tag{4}$$

Histogram fitting techniques can then be used to estimate the unknown conditional densities function's parameters assuming that their form is known. As for each possible value of the threshold $\mathrm{r_T}$ (T ranging from 1 to L), there will exist a new estimation of the unknown probabilities. In [22], the authors suggested to select the threshold that minimizes the criterion function given in (5).

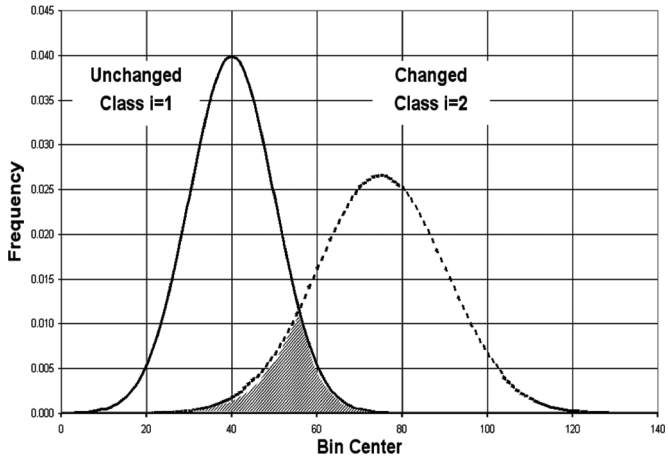

Fig. 2. Change detection: a binary classification problem.

$$J(\mathrm{r_T}) = -\sum_{i=1,2}\left[P_i(\mathrm{r_T}).\ln P_i(\mathrm{r_T}) + \sum_{\mathrm{r}\in i} h(\mathrm{r}) \ln p_i\left(\frac{\mathrm{r}}{\mathrm{r_T}}\right)\right] \tag{5}$$

where $\mathrm{i} = \{1, 2\}$ refers to the no change and change classes respectively. The threshold that minimizes the criterion function is the one that minimizes the probability of classification error. The r_T appeared in the conditional density function and prior probability is used to emphasize that these are estimated for specific threshold value r_T.

In the original minimum error thresholding algorithm, both classes are assumed to have a Gaussian distribution. However, for SAR images this assumption no longer holds. As the accuracy of the method depends on how accurate the statistical model fits the classes, [13] suggested three probability density functions to be used to model the distributions of no change and change classes in the ratio of multitemporal SAR images. In [12], a generalized version of the Gaussian model is used to model the logarithm of the intensity ratio image. The analytical expressions of these statistical models are given in the next section. In this study, the four statistical models were compared.

C. Statistical Models

Log normal distribution: If a random variable is log normally distributed, then its logarithm is normally distributed [32]. Similar to Gaussian distribution this model is defined using two parameters as in (6).

$$p\left(r/\varphi_i, \xi_i^2\right) = \frac{1}{r\xi_i\sqrt{2\pi}} \exp\left(\frac{-(\ln r - \varphi_i)^2}{2\xi_i^2}\right) \tag{6}$$

where $\mathrm{i} = \{1, 2\}$ refers to no change and change classes respectively, φ_i and ξ_i^2 are the first and second order log cumulants defined in (7) for the conditional class's density and r is the random variable.

$$\varphi_i = \frac{\sum_{r\in i} h(r)\ln r}{P_i}, \quad \xi_i^2 = \frac{\sum_{r\in i} h(r)[\ln r - \varphi_i]^2}{P_i} \tag{7}$$

The log normal distribution has the important property of fitting asymmetrical histograms, which makes it more flexible in modeling the distribution of change and no change classes.

Weibull ratio model: assuming each of the multitemporal SAR amplitude images to have a Weibull distribution with the same shape parameter, [13] developed an expression for the probability density function of the SAR amplitude ratio image (8) that depends onto two parameters.

$$p(r/eta, \lambda_i) = \eta_i \lambda_i^{\eta_i} \frac{r^{\eta_i - 1}}{\left(\lambda_i^{\eta_i} + r^{\eta_i}\right)^2} \tag{8}$$

where η_i and λ_i are the distribution parameters and the ratio (r should be greater than 0). The unknown model's parameters are estimated using the method of log cumulants which relate the unknowns to the first and second order log cumulants as in (9).

$$\varphi_i = \log_e \lambda_i, \quad \xi_i^2 = \frac{2\Psi(1,1)}{\eta_i^2} \tag{9}$$

where φ_i and ξ_i^2 are the first and second order log cumulants as defined in (7), and $\Psi()$ is the digamma function. Although this development ignores the correlation between multitemporal images, this model proved to be useful in describing the class's conditional density function.

Nakagami ratio model: similar to Weibull ratio model, this model assumes that, each of the SAR images is Nakagami distributed with the same equivalent number of looks. Image correlation is ignored for simplicity. The probability density function of this model is given in (10).

$$p_i(r/L_i, \gamma_i) = \frac{2\Gamma(2L_i)}{\Gamma^2(L_i)} \frac{\gamma_i^{L_i} \mathrm{r}^{2L_i - 1}}{\left(\gamma_i + \mathrm{r}^2\right)^{2L_i}} \tag{10}$$

where $\mathrm{L_i}$, γ_i are the distribution parameters and Γ is Gamma function. The estimation of the model's parameters is performed by solving (11) which relates the unknown model's parameters to the first and second order log cumulants given in (7).

$$\varphi_i = \frac{\ln \gamma_i}{2}, \quad \xi_i^2 = \frac{\Psi(1, \mathrm{L_i})}{2} \tag{11}$$

Generalized Gaussian model: This model is a generalization of the normal distribution model, with one additional parameter that describes the shape. Varying the shape parameter, generalized Gaussian model can represent a large family of symmetrical distributions among which are the Gaussian, Laplacian and uniform distributions. (12) shows the analytical expression of this model.

$$p\left(r/\mu_i, \sigma_i^2, \alpha_i\right) = a_i \exp\left[-\left(b_i |r - \mu_i|\right)^{\alpha_i}\right]$$
$$\text{where} \quad \mathrm{a_i} = \frac{\mathrm{b_i}\alpha_i}{2\Gamma\left(\frac{1}{\alpha_i}\right)}, \quad \mathrm{b_i} = \frac{1}{\sigma_i}\sqrt{\frac{\Gamma\left(\frac{3}{\alpha_i}\right)}{\Gamma\left(\frac{1}{\alpha_i}\right)}} \tag{12}$$

where μ_i and σ_i are the conventional mean and standard deviation and α_i is the shape parameter. The estimation of the first two parameters is straightforward, while the shape parameter can be estimated by the method described in [33].

In this research, instead of using the model with the logarithmically scaled ratio of the intensity images as suggested by [2], the modified ratio is used since taking the logarithm of the ratio image not only scale the data, but also change its statistical distributional properties [7].

TABLE I
GROUND TRUTH DATA USED IN ACCURACY ASSESSMENT

Group name	No. of pixels Beijing	No. of pixels Shanghai
No Change	1630	1998
Positive Change	1523	2009
Negative Change	711	1199

III. STUDY AREA AND DATA DESCRIPTION

Beijing and Shanghai in China were selected as case studies in this research. As the capital of China, Beijing's active economy and large population are responsible for its faster expansion rate. The total population was estimated to be 19.6 million in 2010 compared to 12.17 million in 1997 and to 9.45 million in 1984 [9]. On the other hand, Shanghai is located in the Yangtze River Delta, Eastern China. This fertile plain is a highly productive agricultural area as well as an area upon which urban growth has rapidly taken place. Shanghai has the largest population (23 millions in 2010) among all Chinese cities. Corresponding to the rapid increase in population, Beijing and Shanghai have witnessed rapid expansion in their built-up areas. Consequently, these two cities witnessed increase in the amount of stress, in the form of waste and pollutant, on the ecosystem [10].

Regarding multitemporal SAR data in Beijing, ENVISAT ASAR C-VV images were acquired on July15, 2008, while one scene of ERS-2 SAR C-VV image from July 19, 1998, a near-anniversary date, was selected to minimize the influence of seasonal changes. As for Shanghai, two scenes of ENVISAT ASAR C-VV images acquired on September 3, 2008 and September 19, 2008 were used in order to cover the whole Shanghai area. One scene of ERS-2 C-VV SAR image acquired on September 7, 1999, a near-anniversary date, was selected for change detection. Both sensors acquire images at 30m spatial resolution. Fieldwork was conducted over Beijing and Shanghai in 2008 and 2009 for validations of the change detection results.

To assess the accuracy, field data, two Landsat images acquired in similar dates to SAR images as well as high-resolution QuickBird images from Google were used. Three different types of samples were selected for accuracy assessment. The first group represented unchanged areas. The second group represented positive changes with backscatter increase while the third group represented negative change with backscatter decrease. Table I shows the number of pixels selected for each group.

IV. RESULTS AND DISCUSSION

The change image was derived with the modified ratio operator using ENVISAT ASAR image from 2008 and the ERS-2 SAR image from 1998 (Beijing) and 1999 (Shanghai) respectively. Then the Kittler-Illingworth algorithm was applied to the modified ratio image histogram to estimate an optimum threshold. Fig. 3 shows the empirical histograms

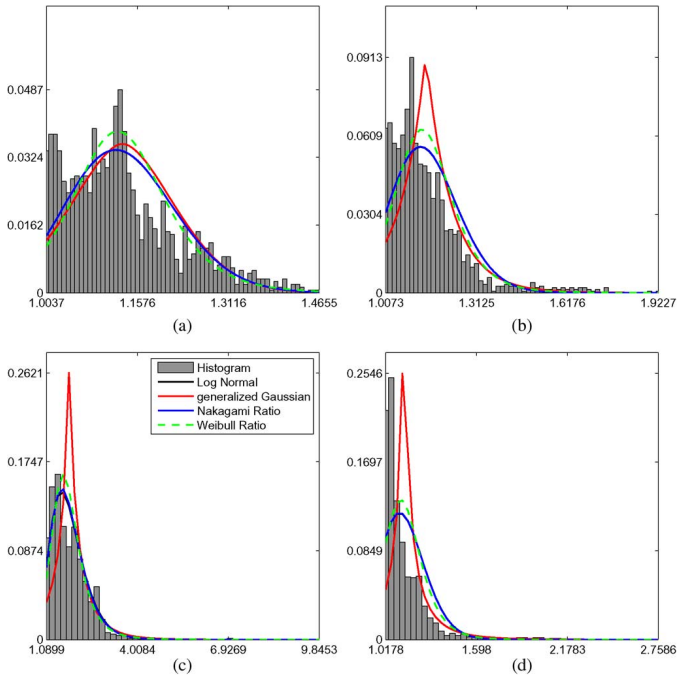

Fig. 3. The histograms of the modified ratio images plotted together with various statistical models for 'change' and 'no-change' class: (a) Beijing 'no-change' class, (b) Beijing 'change' class, (c) Shanghai 'no-change' class, and (d) Shanghai 'change' class.

of the modified ratio images corresponding to (a) Beijing 'no-change' class, (b) Beijing 'change' class, (c) Shanghai 'no-change' class, and (d) Shanghai 'change' class, plotted together with the estimated density functions. The histograms and the density functions were actually estimated at the location of the ground truth data. For the 'change' class in Beijing, the figure clearly shows how the generalized Gaussian and Weibull ratio models slightly overestimate the histogram of the change class. This may indicate that the change result under these two density models will not be as good as that of log normal and Nakagami ratio models. The performances of the estimated density functions are comparable for the 'non-change' class. For both the change and non-change classes in Shanghai, the generalized Gaussian significantly over-estimate the histogram of the change and non-change classes, thus will produce poor results compared with the other density functions. The figure also shows the absolute similarity between the behaviors of log normal and Nakagami ratio models.

The correlation between the various probability density functions and the histogram of the change class are presented in Table II. The correlation between the estimated generalized Gaussian model and the histogram of the change class was the lowest while other models achieved high correlations. Generalized Gaussian is a very flexible density model in term of its ability to fit symmetrical distributions with varying degree of sharpness. However, this model is not suitable to describe the distribution of the change class since its distribution is non-symmetrical.

A. Change Detection Results in Beijing

Table III shows the accuracy assessment of the change results obtained by thresholding the modified ratio image,

TABLE II
CORRELATION COEFFICIENTS BETWEEN THE HISTOGRAM OF THE CHANGE CLASS AND THE ESTIMATED DENSITY FUNCTIONS

Group name	GG	LN	NR	WR
Correlation Coefficient	0.78	0.91	0.91	0.90

TABLE III
CHANGE DETECTION ACCURACY IN BEIJING

Density Model	GG	LN	NR	WR
Positive Change	98.49	92.19	92.19	79.71
Negative Change	84.53	61.32	61.32	52.60
False Alarm	11.23	2.70	2.70	0.18
Overall Error	8.18	11.34	11.34	16.80
Kappa coefficient	0.87	0.82	0.82	0.72
Change %	10.90	5.10	5.10	2.63

assuming generalized Gaussian, log normal, Nakagami ratio, and Weibull ratio as a density models. Even though the generalized Gaussian model achieved the highest Kappa coefficient of agreement (0.87), this model has very high false alarm rate (11%) compared with the solutions under the other three density models. In addition, using the generalized Gaussian model, the algorithm identified very high percentage of the scene as change (11%). This frustrating result is due to the fact that the generalized Gaussian model in not suitable to describe the change/no-change classes with their asymmetrical histograms. On the other hand, log normal and Nakagami ratio models achieved a satisfactory Kappa coefficient (0.82), and a very small false alarm rates (2.7%) compared with that obtained under the generalized Gaussian model. The solution under the Weibull ratio model has a very small false alarm rate (0.18%) due to the relatively poor detection accuracy. The detection accuracy in areas characterized by increase in backscatter coefficient over time is satisfactory in general. This is true for all models except for the Weibull distribution that achieved moderate detection accuracy. Weibull ratio has a very low discrimination capability between the classes, which is responsible for the under-estimation of the changed areas.

The detected change maps are shown in Fig. 4. Positive and negative changes are shown in yellow and blue respectively overlaid in a false color composite created using the multitemporal images. The area to the right is Beijing international airport, where a lot of positive change (new building) and negative change (new runways and golf courses) has been constructed after the 1998 image was acquired. It is evident that the algorithm managed to identify many changed areas successfully.

For the identification of new built-up areas, i.e. areas with backscatter increase, the results indicate that the log normal and Nakagami ratio models with the modified ratio image achieved the best result since they have very high detection accuracies in positive change areas and at the same time have low false alarm rates. For the identification of negative changes, the algorithm did not perform well and the percentage of the negative

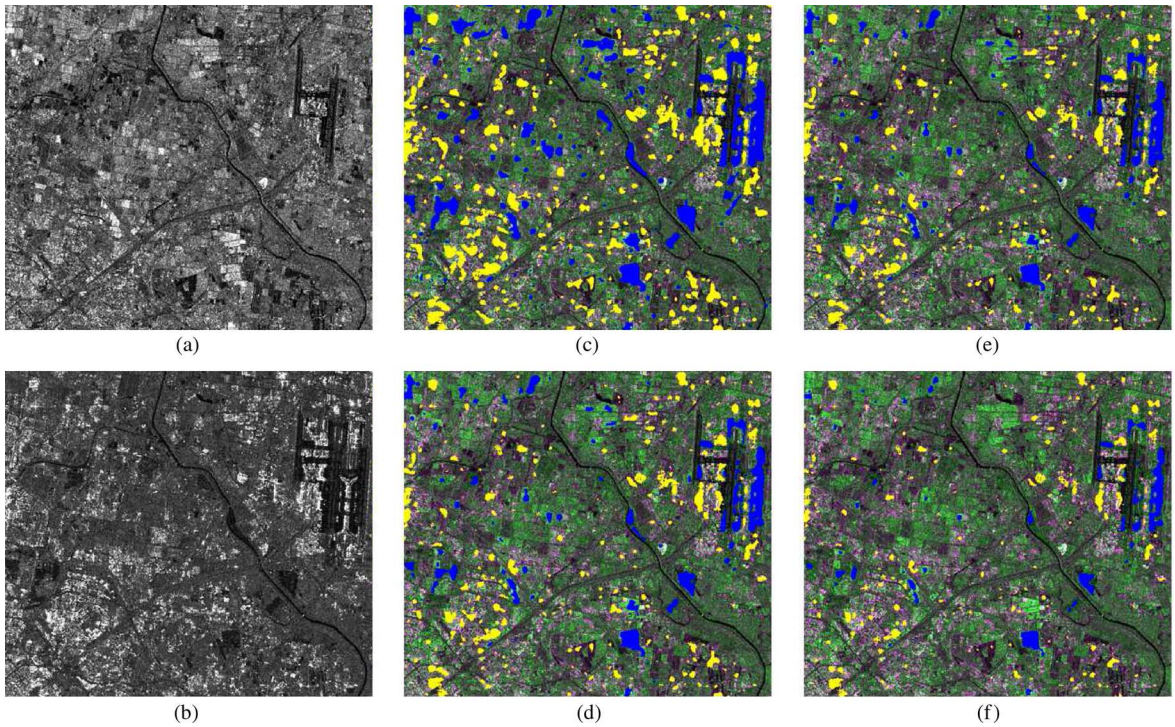

Fig. 4. (a) Date one image, (b) Date two image, and the detected positive (yellow) and negative (blue) changes in Beijing overlaid in a false color composite using (c) GG, (d) LN, (e) NR, and (f) WR.

changed detected is 61.32%. This can be attributed to the low intensity of changes (as measured from the change variable) in the areas where the backscatter has decreased compared with the very high intensity of changes in areas where the backscatter has increased. This occurred because the changes in the scene are dominated by new built-up areas with strong increase in the radar backscatter over time. Even though the negative change detection accuracy is rather low, the algorithm can effectively identify the major negative changes as demonstrated in Fig. 4. It is obvious that many of the newly constructed airport runways and golf courses were correctly identified.

B. Change Detection Results in Shanghai

The change detection accuracies obtained in Shanghai are presented in Table IV. Similarly, the generalized Gaussian model surpassed all other models in term of Kappa coefficient, positive change detection accuracy, negative change detection accuracy and the overall accuracy. Again, theses high accuracies were achieved at the expenses of considerably high false alarm rate. This is mainly because this model misrepresents the distribution of change class as reflected by its low correlation coefficient shown in Table II. As a result, the generalized Gaussian model identifies high percentage of the scene as changed (11.6%) compared to the log normal and Nakagami ratio models (5%). Yet the differences between the detection accuracies in positive change areas between these models are negligible. Therefore it can be concluded the total change percentage under this model is overestimated.

Similar to Beijing results, Nakagami ratio and log normal models achieved very good detection accuracy in positive change areas and also have noticeably smaller false alarm rates.

TABLE IV
CHANGE DETECTION ACCURACY IN SHANGHAI

Density Model	GG	LN	NR	WR
Positive Change	85.27	81.68	82.03	79.69
Negative Change	80.90	55.80	57.46	42.54
False Alarm	9.86	4.61	4.75	3.35
Overall Error	13.87	19.02	18.56	22.36
Kappa coefficient	0.75	0.70	0.71	0.65
Change %	11.56	5.00	5.00	3.07

But the main weakness of these two models is their lower detection accuracies in areas where the backscatter decreased over time. Weibull density function yielded the lowest accuracies.

Fig. 5 shows the detected positive and negative changes in yellow and blue respectively, draped over a false color composite of SAR data over Shanghai. It is apparent that with the modified ratio operator, the algorithm managed to successfully identify many of the changed areas.

V. CONCLUSION

In this research, the effectiveness of the minimum-error thresholding algorithm in identifying urban changes in Beijing and Shanghai was evaluated. For the comparison of the multitemporal SAR images, the modified ratio operator was developed. This operator has the important property of considering both positive and negative changes simultaneously. As a result, this operator increases the size of the change class which in turn improves the accuracy of the estimation of the optimum threshold. Four different probability density models were tested

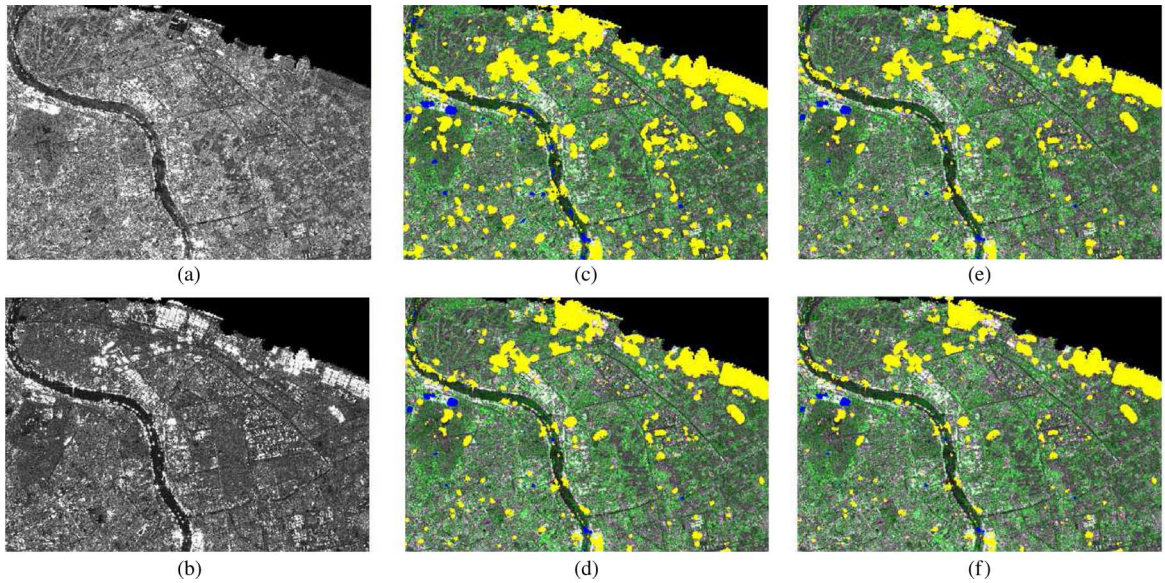

Fig. 5. (a) Date one image, (b) Date two image, and the detected positive (yellow) and negative (blue) changes in Shanghai overlaid in a false color composite using (c) GG, (d) LN, (e) NR, and (f) WR.

to model the distributions of the change and no-change classes in the modified ratio image. These models are the generalized Gaussian, log normal, Nakagami ratio, and Weibull ratio models. The best change results are obtained by using either log normal or Nakagami ratio to model the change/no-change classes. The positive change detection accuracies were very good in general except for the Weibull ratio model while negative change accuracies were poor. This is mainly due to the low intensity of change in these areas compared with the very high intensity of change found in positive change areas. Further research is planned to incorporate contextual information in the change detection analysis by using Markov Random Field to model the interdependencies of pixels.

ACKNOWLEDGMENT

The authors would like to thank the European Space Agency (ESA) for the ENVISAT and ERS-2 SAR data.

REFERENCES

[1] World Population Prospects: The 2010 Revision. United Nations, New York, 2011.
[2] E. H. Wilson *et al.*, "Development of a geospatial model to quantify, describe and map urban growth," *Remote Sens. Environ.*, vol. 86, no. 3, pp. 275–285, 2003.
[3] Q. Zhang, Y. Ban, J. Liu, and Y. Hu, "Simulation and analysis of urban growth scenarios for the greater Shanghai area, China," *Computers, Environment and Urban Systems*, vol. 35, no. 2, pp. 126–139, 2011.
[4] J. Chen, P. Gong, C. He, R. Pu, and P. Shi, "Land-use/land-cover change detection using improved change-vector analysis," *Photogramm. Eng. Remote Sens.*, vol. 69, no. 4, pp. 369–379, 2003.
[5] S. Chen, S. Zeng, and C. Xie, "Remote sensing and GIS for urban growth analysis in China," *Photogramm. Eng. Remote Sens.*, vol. 66, no. 5, pp. 593–598, 2000.
[6] C. He, A. Wei, P. Shi, Q. Zhang, and Y. Zhao, "Detecting land-use/land-cover change in rural-urban fringe areas using extended change-vector analysis," *Int. J. Appl. Earth Observ. Geoinf.*, vol. 13, no. 4, pp. 572–585, 2011.
[7] W. Su, J. Li, Y. Chen, Z. Liu, J. Zhang, T. Low, and I. Suppiah *et al.*, "Textural and local spatial statistics for the object-oriented classification of urban areas using high resolution imagery," *Int. J. Remote Sens.*, vol. 29, no. 11, pp. 3105–3117, 2008.
[8] Q. Zhang, J. Wang, P. Gong, and P. Shi, "Study of urban spatial patterns from SPOT panchromatic imagery using textural analysis," *Int. J. Remote Sens.*, vol. 24, no. 21, pp. 4137–4160, 2003.
[9] Q. Zhang, J. Wang, X. Peng, P. Gong, and P. Shi, "Urban built-up land change detection with road density and spectral information from multi-temporal Landsat TM data," *Int. J. Remote Sens.*, vol. 23, no. 15, pp. 3057–3078, 2002.
[10] Q. Zhang, Y. Ban, Y. Hu, and J. Liu, "The trajectories of urban land and industrial land in Shanghai over the past 30 years," in *Proc. Urban Remote Sensing Joint Event*, Shanghai, China, 2009.
[11] E.-M. Rignot and J. J. Van Zyl, "Change detection techniques for ERS-1 SAR data," *IEEE Trans. Geosci. Remote Sens.*, vol. 31, no. 4, pp. 896–906, 1993.
[12] Y. Bazi, L. Bruzzone, and F. Melgani, "An unsupervised approach based on the generalized Gaussian model to automatic change detection in multitemporal SAR images," *IEEE Trans. Geosci. Remote Sens.*, vol. 43, no. 4, pp. 874–887, 2005.
[13] G. Moser and S. B. Serpico, "Generalized minimum-error thresholding for unsupervised change detection from SAR amplitude imagery," *IEEE Trans. Geosci. Remote Sens.*, vol. 44, no. 10, pp. 2972–2982, 2006.
[14] F. Bujor, J.-M. Nicolas, E. Trouve, and J.-P. Rudant, "Application of log-cumulants to change detection in multi-temporal SAR images," in *Proc. IEEE Geosci. Remote Sens. (IGARSS'03)*, 2003, pp. 1386–1388.
[15] P. Gamba, F. Dell'Acqua, and G. Lisini, "Change detection of multitemporal SAR data in urban areas combining feature-based and pixel-based techniques," *IEEE Trans. Geosci. Remote Sens.*, vol. 44, no. 10, pp. 2820–2827, 2006.
[16] Y. Ban and H. Hu, "Multitemporal RADARSAT-1 fine-beam SAR data for land-cover mapping and change detection," in *Proc. Urban Remote Sensing Joint Event*, Paris, France, 2007.
[17] D. Perissin and T. Wang, "Time-series InSAR applications over urban areas in China," *IEEE J. Sel. Topics Appl. Earth Observ. Remote Sens. (JSTARS)*, vol. 4, no. 1, pp. 92–100, 2011.
[18] O. Adam and Y. Ban, "Multitemporal spaceborne SAR data for change detection in urban areas: A case study in Shanghai," in *Proc. ISPRS VCGVA*, Wuhan, China, 2009.
[19] J. Inglada and G. Mercier, "A new statistical similarity measure for change detection in multitemporal SAR images and its extension to multiscale change analysis," *IEEE Trans. Geosci. Remote Sens.*, vol. 45, no. 5, pp. 1432–1445, 2007.
[20] R. J. Dekker, "Speckle filtering in satellite SAR change detection imagery," *Int. J. Remote Sens.*, vol. 19, no. 6, pp. 1133–1146, 1998.
[21] F. Melgani, G. Moser, and S. B. Serpico, "Unsupervised change-detection methods for remote-sensing images," *Opt. Eng.*, vol. 41, no. 12, pp. 3288–3297, 2002.
[22] J. Kittler and J. Illingworth, "Minimum error thresholding," *Pattern Recogn.*, vol. 19, no. 1, pp. 41–47, 1986.

[23] F. Wu, C. Wang, H. Zhang, and B. Zhang, "Change detection and analysis with Radarsat-1 SAR image," in *Proc. IEEE Int. Geosci. Remote Sens. Symp. (IGARSS'07)*, 2007.
[24] Y. Bazi, L. Bruzzone, and F. Melgani, "Automatic identification of the number and values of decision thresholds in the log-ratio image for change detection in SAR images," *IEEE Trans. Geosci. Remote Sens.*, vol. 3, no. 3, p. 3491-353, 2006.
[25] M. Gong, Y. Cao, and Q. Wu, "A neighborhood-based ratio approach for change detection in SAR images," *IEEE Geosci. Remote Sens. Lett.*, vol. 9, no. 2, pp. 307–311, 2012.
[26] F. Bovolo and L. Bruzzone, "A detail-preserving scale-driven approach to change detection in multitemporal SAR images," *IEEE Trans. Geosci. Remote Sens.*, vol. 43, no. 12, pp. 2963–2972, 2005.
[27] G. Moser, S. Serpico, and G. Vernazza, "Unsupervised change detection from multichannel SAR images," *IEEE Geosci. Remote Sens. Lett.*, vol. 4, no. 2, pp. 278–282, 2007.
[28] C. Carincotte, S. Derrode, and S. Bourennane, "Unsupervised change detection on SAR images using fuzzy hidden Markov chains," *IEEE Trans. Geosci. Remote Sens.*, vol. 44, no. 2, pp. 432–441, 2006.
[29] M. Liao, L. Jiang, H. Lin, Huang, and J. Gong, "Urban change detection based on coherence and intensity characteristics of SAR imagery," *Photogramm. Eng. Remote Sens.*, vol. 74, no. 8, pp. 999–1006, 2008.
[30] B. Xiong, Q. Chen, Y. Jiang, and G. Kuang, "A threshold selection method using two SAR change detection measures based on the Markov random field model," *IEEE Geosci. Remote Sens. Lett.*, vol. 9, no. 2, pp. 287–291, 2012.
[31] R. O. Duda, P. E. Hart, and D. G. Stork, *Pattern Classification*. New York: Wiley, China Machine Press, 2001.
[32] B. W. Lindgren, *Statistical Theory*. London, UK: Collier-Macmillan, 1968.
[33] K. Sharifi and A. Leon-Garcia, "Estimation of shape parameter for generalized Gaussian distribution in subband decomposition of video," *IEEE Trans. Circuits Syst. Video Technol.*, vol. 5, no. 1, pp. 52–56, 1995.

Yifang Ban (M'02) received the B.Sc. (honours) in computer cartography and the M.Sc. in remote sensing from Nanjing University, China, in 1984 and 1987, respectively. She received the Ph.D. in remote sensing from the University of Waterloo, Canada, in 1996. She received various scholarships and awards in China and Canada.

Since 2004, she has been the Chair Professor of Geoinformatics of the Department of Urban Planning and Environment at the Royal Institute of Technology–KTH in Stockholm, Sweden. Before joining KTH, she was a tenured Associate Professor at York University in Toronto, Canada. She was an Assistant Professor at Stockholm University during 1998–2000 and a Senior Research Engineer at KTH during 1996–1997 in Stockholm, Sweden. She was a Remote Sensing Consultant at Watts, Griffis and Mcquat Ltd. (1995–1996) and a GIS Analyst at PDM Information Technology Inc. (1991–92) in Toronto, Canada. Her current research interests include SAR image analysis and classification, image segmentation, multisensor data fusion, urban land-cover mapping and change detection.

Prof. Ban is the Swedish Representative to EARSeL and co-chair of the EARSeL Special Interest Group "Temporal Analysis of Satellite Images". She is a reviewer for several international journals.

Osama A. Yousif received the B.Sc. degree in surveying engineering from the University of Khartoum, Sudan, the M.Sc. degree in geodesy from Sudan University of Science and Technology, Sudan, and the M.Sc. in geodesy and geoinformatics in 2009 from the Royal Institute of Technology–KTH, Stockholm, Sweden. Currently, he is pursuing the Ph.D. degree in geoinformatics at KTH.

His main area of research is change detection using SAR and optical remote sensing images.